KSME

Springer

Journal of Mechanical Science and Technology 34 (4) 2020

Original Article
DOI 10.1007/s12206-020-0333-y

Keywords:
· High speed on/off valve
· Adaptive PWM control
· Dynamic performance
· Energy efficiency
· Feedback

Correspondence to:
Yuchuan Zhu
meeyczhu@nuaa.edu.cn

Citation:
Gao, Q., Zhu, Y., Luo, Z., Bruno, N. (2020). Investigation on adaptive pulse width modulation control for high speed on/off valve. Journal of Mechanical Science and Technology 34 (4) (2020) 1711~1722.
http://doi.org/10.1007/s12206-020-0333-y

Received April 23rd, 2019
Revised December 24th, 2019
Accepted February 7th, 2020

† Recommended by Editor
Ja Choon Koo

Investigation on adaptive pulse width modulation control for high speed on/off valve

Qiang Gao, Yuchuan Zhu, Zhang Luo and Niyomwungeri Bruno

National Key Laboratory of Science and Technology on Helicopter Transmission, Nanjing University of Aeronautics and Astronautics, Nanjing, China

Abstract High speed on/off valves (HSV) have often been used to control flow or pressure in digital hydraulic systems due to higher switching frequency. However, the dynamic performance and energy efficiency are highly affected by the supply pressure and the carrier frequency. In this paper, a new adaptive PWM control method for HSV based on software is proposed. The proposed adaptive PWM consists of a reference PWM, an excitation PWM, a high frequency PWM, and a reverse PWM. First, the nonlinear model of the HSV was established, and the structural composition and working principle of the proposed adaptive PWM control strategy were presented. Secondly, individual feedback controllers for the excitation PWM, the high frequency PWM, and the reverse PWM were designed, respectively; and each of the individual feedback controllers was experimentally verified. Finally, the comparative experimental results demonstrated that, with the proposed adaptive PWM control, the rising delay time of the control pressure drastically reduces by 84.6 % (from 13 ms to 2 ms), the duty cycle's effective range remains large (12 %-85 %) even with high carrier frequency (100 Hz), and the temperature rise of the valve's coil shell is reduced by 61.5 %, compared to the three-voltage control. In addition, the dynamic performance and the energy efficiency of the HSV are not affected by the supply pressures and carrier frequencies, which proves that the proposed control strategy can improve the robustness and stability of the valve system.

1. Introduction

The conventional electro-hydraulic servo system (EHSS) has been extensively employed in various applications, such as robots, aircraft actuators, aero-engine and so on, by utilizing the advantages of its small size-to-power ratio and high frequency response [1, 2]. Servo valve used as the control component of EHSS has disadvantages of high power consumption and low reliability due to high sensitivity to oil contamination [3]. There exist problems such as null shift and jam in servo valve, especially working in an environment with high temperature, high pressure, and strong shock.

A digital hydraulic system offers high potential for innovative technologies, which is considered as a competitive alternative to EHSS due to its high efficiency and high reliability [4, 5]. Another advantage of the digital hydraulic system is its ability to implement "intelligence" (such as intelligent monitoring and fault diagnosis) using simple, robust hardware. Hence, the digital hydraulic system is capable of "plug and play" and fit for industry 4.0 requirements [6].

Generally, a digital hydraulic system uses a combination of high speed on/off valves (HSV) controlled by different control methods, such as pulse width modulation (PWM), pulse frequency modulation (PFM), pulse code modulation (PCM) and pulse number modulation (PNM) [7-9]. HSV have the possibility of zero leakage due to two working states: On or off. Compared with the servo valve, HSV have several benefits, including high efficiency, high reliability and robustness [10, 11]. Moreover, HSV have been employed in sundry applications, such as aircraft brake systems [12], antilock braking systems (ABS) [13], construction machines [14] and

so on. However, HSV still need to improve to meet the requirements of the digital hydraulic servo system, such as higher switching frequency and lower power consumption. Recently, researchers have focused on structure optimization, new electro-mechanical converter, and control strategy.

With respect to structure optimization of HSV, Wu et al. [1] designed a hollow plunger type solenoid for HSV by multi-objective particle swarm optimization method. The experimental results indicate that the opening and closing time of the solenoid valve are 2.4 ms and 2 ms, respectively. Man et al. [15] presented a novel high-speed electromagnetic actuator by utilizing permanent-magnet shielding, which can help increase the flux of main magnetic path. The experiments indicate that the closing and opening time of the actuator reach 2.24 ms and 7.78 ms under displacement of 0.6 mm, respectively. Kong et al. [16] proposed a new structure of solenoid with parallel coils. In the study, the closing and opening time of the solenoid with parallel coils were shortened by 75.8 % and 70.5 %, compared with a solenoid with a single coil. However, the structure optimization is just adaptable in the design stage of HSV because the process involves partial or complete change of the structure and manufacturing of new prototypes to validate it.

Additionally, some new electro-mechanical converters have been developed to shorten the opening and closing time of HSV. These electro-mechanical converters are actuated by materials, such as giant magnetostrictive material [17], piezoelectric [18, 19] and other soft magnetic materials [20] with the advantages of quick response and small size. However, the application of HSV actuated by these smart materials is limited by high cost and small output displacement.

Therefore, compared with both aforementioned solutions, control strategy optimization can at the same time improve dynamic performance and energy efficiency. Also, it is easy to implement with no structural changes, especially in existing HSV. For example, Cheng et al. [21] verified that different control methods have different influence on power consumption and dynamic performance of HSV using finite element numerical simulation. Goraj [22] studied the influence of PWM control on the temperature distribution in the armature. Zhao [23, 24] demonstrated that the design criteria of control method should take into account both dynamic performance and energy efficiency.

Nowadays, multiple voltage source control methods are used in HSV to improve dynamic performance and energy efficiency [25]. Lee [26] designed and manufactured an electronic valve driving circuit with fast response characteristics by using a three-power source. Plöckinger et al. [27] proposed a double voltage control signal in which a boost voltage is used to get a higher current to drive the coil and a low voltage is used to obtain the hold current. Linjama et al. [28] designed an AC booster power electronic circuit to drive parallel on/off valves. The circuit provides high current peak to open a valve by using 220 uF boost capacitor and low holding voltage to maintain the valve open. Zhong et al. [29, 30] proposed a three power source excitation control algorithm based on current feedback.

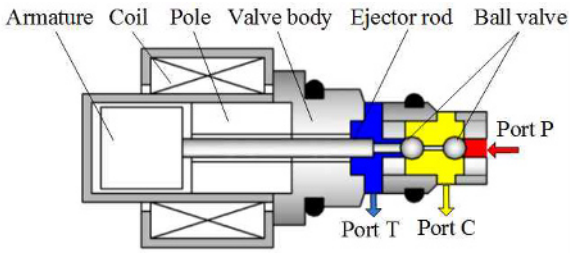

Fig. 1. Schematic diagram of the HSV.

In the study, a high positive voltage and a low positive voltage were used in opening and fully-open holding stage of HSV, and a high negative voltage was employed in the closing stage of HSV. The experimental results indicate that the opening and closing time of the solenoid are shortened by 35.3 % and 25.0 %, respectively, and the average energy consumption is reduced by 70.4 %. Therefore, multiple voltage source control can meet the requirements of HSV with high dynamic performance and energy efficiency. However, it is difficult to implement in many practical applications, such as aero-engine and vehicle, due to the need for multiple voltage sources.

The purpose of this study was to develop a new PWM control method for HSV to meet the requirements of the digital hydraulic system. In this paper, a software-based adaptive PWM control method is proposed which consists of reference PWM, excitation PWM, high frequency PWM and reverse PWM. The word “adaptive” refers to the ability of the proposed control method to maintain the same dynamic performances of the HSV under different supply pressures and the carrier frequencies. First, a nonlinear model of HSV is presented. Secondly, the structural composition and working principle of the proposed adaptive PWM control method are given. Moreover, individual feedback controllers for the excitation PWM, the high frequency PWM, and the reverse PWM are proposed to ensure that dynamic performance and energy efficiency are not affected by the supply pressure and carrier frequency. Finally, the experimental results indicate that the proposed adaptive PWM control method has better dynamic and static performance, and lower energy consumption compared with the three-voltage control method.

2. Mathematical model of HSV

In this research, a 2-position and 3-way HSV (Guizhou Honglin HSV3102S3) was used as a study object as shown in Fig. 1. The rated flow of the HSV is 9 L/min under a rated supply pressure of 10 MPa. Initially, when the coil is de-energized, the ball is moved to the left side by the high pressure from port P. In that case, port C is connected to port P and port T is blocked. Conversely, when the coil is energized, the ball is moved to the right side by the electromagnetic force. In that case, port C is connected to port T and port P is blocked. Therefore, the pressure at port C is used to assess the dynamic performance of the HSV because it can reflect the

movement of the ball valve.

2.1 Electromagnetic model

Assuming that the magnetic flux is uniformly distributed in the medium, a magnetic circuit equation can be defined as follows [31]:

$$NI = (H_c L_c + H_g L_g) k_f = H_c L_{eq} k_f \tag{1}$$

where N is the number of coil turns; I is coil current; H_c, H_g are the equivalent magnetic field intensity in the core and in the air gap, respectively; L_c and L_g are the equivalent length of the magnetic circuit inside the core and air gap, respectively; L_{eq} is the equivalent length of the whole magnetic circuit; k_f is the leakage magnetic coefficient.

The expression of the L_{eq} is defined as:

$$L_{eq} = L_c + u_r (L_0 - x_v) \tag{2}$$

where u_r is the core relative permeability; L_0 and x_v are the initial length of the air gap and the displacement of ball valve, respectively.

The relationship among H_c, φ and L is as follows:

$$H_c = \frac{B}{u_c} = \frac{\varphi}{u_c S} \tag{3}$$

$$LI = N\varphi = \psi \tag{4}$$

where φ is the magnetic flux; B is the magnetic flux density; S is the effective sectional area of the armature; u_c is the core permeability; ψ is flux linkage.

The coil inductance L is obtained from Eqs. (1)-(4) as follows:

$$L = \frac{N^2 u_c S}{L_{eq}} = \frac{N^2 \mu_0 S}{(L_c / u_r + (L_0 - x_v)) k_f} \tag{5}$$

where μ_0 is air permeability.

Based on Kirchhoff's law of voltage, the balance equation of coil voltage is as follows:

$$U = IR + L\frac{\mathrm{d}I}{\mathrm{d}t} + I\frac{\mathrm{d}L}{\mathrm{d}t} \tag{6}$$

where U and R are the driving voltage and equivalent resistance of the coil. The derivative of L is as follows:

$$\frac{\mathrm{d}L}{\mathrm{d}t} = \frac{N^2 I^2 \mu_0 S}{(L_c / u_r + (L_0 - x_v))^2 k_f^2} \frac{\mathrm{d}x_v}{\mathrm{d}t} \tag{7}$$

The electromagnetic force F_m is as follows:

$$F_m = \frac{\psi^2}{2N^2 \mu_0 S} \tag{8}$$

The problem of temperature rise is pervasive in HSV due to the fully-open holding current, which may lead to unnecessary power consumption. The average thermal power equation of the coil in one period is as follows:

$$P = \frac{\sum_{x=0}^{n} I^2 R t_x}{\sum_{x=0}^{n} t_x} \tag{9}$$

where P is the average thermal power of coil. The temperature rise of the coil is written as:

$$\Delta t = \frac{\rho(1 - e^{-t/T_r})}{2k_t fb} \left(\frac{NI}{l}\right)^2 \tag{10}$$

The heat extraction coefficient relates to the heat radiation area and the temperature rise. The empirical equation of heat extraction coefficient is as follows [32]:

$$k_t = \frac{24.5}{\sqrt[3]{A}} (1 + 0.012\Delta t) \tag{11}$$

$$A = \pi l (D_1 + D_2) \tag{12}$$

where ρ is the resistivity of the coil; k_t is heat extraction coefficient; T_r is time constant; b, l are the width and height of the coil, respectively; A is the heat radiation area; D_1 and D_2 are inner diameter and the outer diameter of the coil, respectively.

2.2 Dynamical model of the ball valve

The force balance equation of the ball valve can be described by

$$m_v \ddot{x}_v = F_m - p_s A_s - B_v \dot{x}_v - F_y \tag{13}$$

where m_v is the mass of the ball valve; B_v is the movement damping of the ball valve; p_s is the pressure of port P; A_s is the effective area of port P, and F_y is the steady flow force.

2.3 State-space equation of HSV

Based on the aforementioned equations, a state space representation of the HSV can be formulated as shown in Eq. (15). U is defined as input variable; I is defined as output variable because it is detectable. The state variables of the system are defined as follows:

$$x_1 = x_v, \quad x_2 = \dot{x}_v, \quad x_3 = \psi \tag{14}$$

The system can be expressed in a state-space form as:

Table 1. Related parameters of HSV.

Name	Unit	Symbol	Value
Mass of ball valve	g	m_v	10
Air permeability	H/m	μ_0	$4\pi\times10^{-7}$
Number of coil turns	-	N	900
Resistance of the coil	Ω	R	10.2
Initial length of gap	mm	L_0	0.45
Inner diameter of the coil	mm	D_1	10
Outer diameter of the coil	mm	D_2	24
Height of the coil	mm	l	17
Width of the coil	mm	b	2
The filling coefficient of the coil	-	f_t	0.58
The time constant of the coil	-	T_r	700
The resistivity of the coil	Ω·m	ρ	1.75e-8

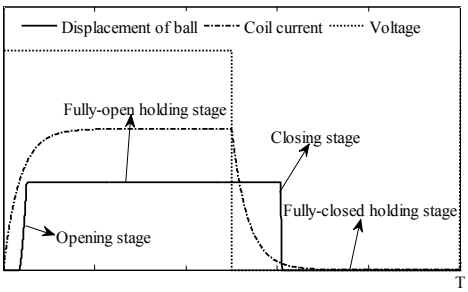

Fig. 2. Working process of HSV.

$$\begin{cases} \dot{x}_1 = x_2 \\ m_v\dot{x}_2 = F_m - p_s A_s - F_y - B_v x_2 \\ \dot{x}_3 = U - R\dfrac{x_3}{L} \\ I = \dfrac{x_3}{L} \end{cases} \tag{15}$$

The main parameters of the HSV are shown in Table 1. Some of the parameters are measured and others refer to Refs. [30, 32].

3. Mathematical model of the valve

Nowadays, HSV are driven by a single PWM signal. As shown in Fig. 2, the working process of HSV can be divided into four stages: Opening stage, fully-open holding stage, closing stage, and fully-closed holding stage. However, the disadvantages of a single PWM control method include high power consumption due to maximum current during the fully-open holding stage and larger delay time of valve due to inductance during the closing stage. Consequently, the single PWM control has become more and more difficult to satisfy the increasing exacting performance demands in terms of high switching frequency and low power consumption in many practical applications.

A control strategy of multiple voltage sources can improve the switching frequency and energy efficiency of HSV, but the cost and size of the system are sacrificed.

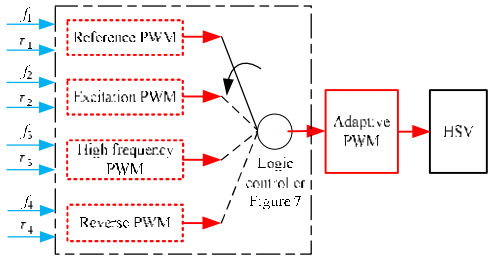

Fig. 3. Composition of the adaptive PWM signal.

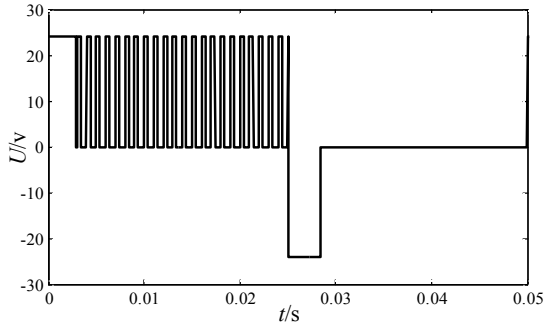

Fig. 4. Adaptive PWM signal.

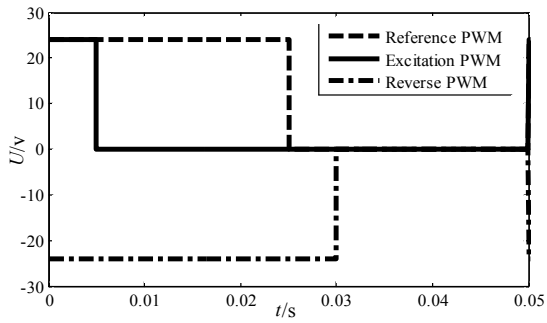

Fig. 5. Reference PWM, excitation PWM, and reverse PWM.

3.1 Structural composition

From the viewpoint of the mechanism of signal generation, this paper proposed a new adaptive PWM control strategy as shown in Fig. 3.

As shown in Fig. 3, the adaptive PWM consists of four different functional signals based on software logic controller: Reference PWM, excitation PWM, high frequency PWM, and reverse PWM. Each PWM signal has its own duty cycle and carrier frequency. An example of an adaptive PWM signal is shown in Fig. 4, and it also can be obtained by multiple voltage source control method [30].

Fig. 5 shows the relationship among reference PWM, excitation PWM and reverse PWM in one period (For example f_1 = 20 Hz). The carrier frequency f_2 of the excitation PWM and f_4 of the reverse PWM are determined by the carrier frequency f_1 of

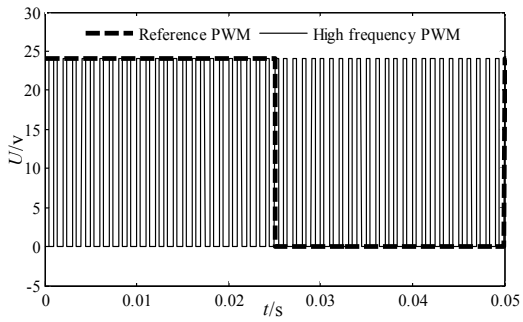

Fig. 6. Reference PWM and high frequency PWM.

reference PWM, which defines the switching frequency of HSV.

The duty cycle τ_1 of reference PWM is used to control the average output flow rate of HSV. The duty cycle τ_2 of excitation PWM and duty cycle τ_4 of reverse PWM are used to control the energizing time and de-energizing time of the coil, respectively. Fig. 6 shows the relationship between reference PWM and high frequency PWM in one period.

It can be seen that the carrier frequency of the high frequency PWM is comparatively higher than the carrier frequency of the reference PWM. The carrier frequency f_3 and duty cycle τ_3 of high frequency PWM are used to optimize the fluctuation and value of coil current, respectively. But due to the limitation of the controller, the carrier frequency f_3 can only reach 1 kHz.

3.2 Working principle

The working principle flowchart of the adaptive PWM control strategy is shown in Fig. 7, in which the oil current I, the inlet pressure p_s and the estimation of the displacement x_v are feedback variables of the adaptive PWM controller. In addition, the coil current I and inlet pressure p_s are both collected data and the value of the displacement x_v is estimated by the sliding mode observer.

Initially, the excitation PWM works to drive the ball valve movement when the rising edge of the reference PWM is detected. When the ball valve reaches the maximum opening, high frequency PWM works instead of excitation PWM. The duty cycle τ_3 of the high frequency is controlled based on the feedback of supply pressure. When the falling edge of reference PWM is detected, the reverse PWM works to decrease coil current forcefully to reduce the closing time. Finally, when the coil current drops to 0, the reference PWM which is 0 at this stage drives the HSV.

Based on the described working principle, the carrier frequency and duty cycle of each PWM signal are the controllable parameters. The carrier frequency (f_1) and the duty cycle (τ_1) of the PWM are determined by the user or working conditions, which affect the switching characteristics of the HSV. In addition, the carrier frequency (f_1) has some influences on the dynamic performance and energy efficiency because the inductance of the coil varies under different carrier frequencies. To

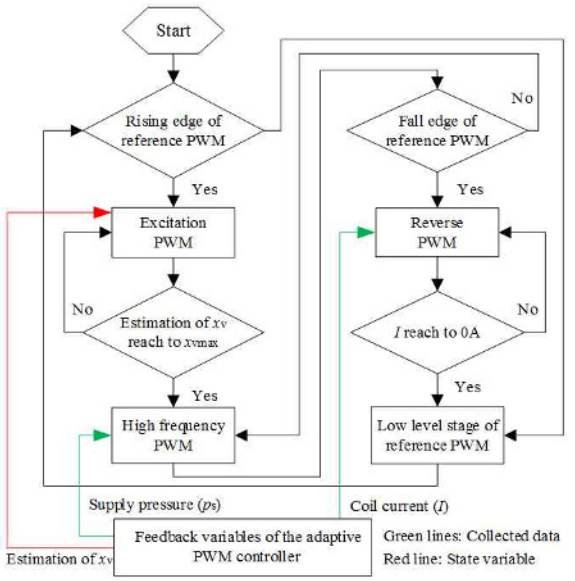

Fig. 7. Flowchart of the adaptive PWM.

compensate the effects of carrier frequency on dynamic performance and energy efficiency, three duty cycles (τ_2, τ_3 and τ_4) are adaptively controlled.

4. Design and verification of the adaptive PWM

4.1 Excitation PWM

Excitation PWM is used in the opening stage. The increase of the supply pressure increases the motion resistance of the ball valve. Therefore, the supply pressure has a great influence on the duty cycle τ_2 which is used to ensure that the valve can move to the maximum opening.

To overcome the influence of the supply pressure, this paper proposed a controller for τ_2 based on sliding mode observer in which τ_2 is calculated using the ball moving time t_1.

$$\tau_2 = \tau_1 + t_1 f_1 \tag{16}$$

where t_1 denotes the time period in which the ball valve moves from 0 to maximum opening.

The nonlinear system of HSV is observable because its gram matrix is nonsingular [33]. So, the sliding mode observer can be designed. The displacement of HSV is estimated by the measurement of the coil current and its sliding mode observer is defined as:

$$\begin{cases} \dot{\hat{x}}_1 = \hat{x}_2 - h_1 s - M_1 \operatorname{sgn}(s) \\ \dot{\hat{x}}_2 = \dfrac{1}{m_v}\left[\dfrac{\hat{\psi}^2}{2N^2\mu_0 S} - p_s A_s - F_y - B_v \hat{x}_2\right] - h_2 s - M_2 \operatorname{sgn}(s) \end{cases} \tag{17}$$

Then

$$\hat{\psi} = \int_0^t U - R\frac{x_3}{L}dt + \psi(0) \tag{18}$$

where $\hat{x}_1$ and $\hat{x}_2$ are the estimated displacement and the estimated velocity of ball valve, respectively; h_1, h_2, M_1 and M_2 are positive gain constant, respectively; and sgn( ) is defined as

$$\mathrm{sgn}(s) = \begin{cases} +1 & s > 0 \\ -1 & s < 0 \end{cases} \tag{19}$$

The error of coil current is defined as the surface of sliding mode observer as follows:

$$s = \hat{I} - I = \frac{\hat{\psi}}{\hat{L}} - I \tag{20}$$

Let $\tilde{x}$ ($\tilde{x} = \hat{x} - x$) denote the estimation error, its state equations is as follows:

$$\begin{cases} \dot{\tilde{x}}_1 = \tilde{x}_2 - h_1 s - M_1 \mathrm{sgn}(s) \\ \dot{\tilde{x}}_2 = \dfrac{1}{m_v}\left[\dfrac{\hat{\psi}^2 - \psi^2}{2N^2\mu_0 S} - B_v\tilde{x}_2\right] - h_2 s - M_2 \mathrm{sgn}(s) \end{cases} \tag{21}$$

From Eqs. (6)-(8) and (17), the following equations can be deduced:

$$\frac{\mathrm{d}L}{\mathrm{d}x} = \frac{N^2\mu_0 S k_f}{(L_c/u_r + (L_0 - x_v))^2 k_f^2} > 0 \tag{22}$$

According to Eqs. (7), (21) and (22), we can infer that $L(\hat{x}) < L(x)$, $\hat{I} < I$, $s < 0$, $\dot{\tilde{x}} > 0$, $\dot{s} > 0$, and $s\dot{s} < 0$, when $\hat{x} - x < 0$. Conversely, we can infer that $L(\hat{x}) > L(x)$, $\hat{I} > I$, $s > 0$, $\dot{\tilde{x}} < 0$, $\dot{s} < 0$, when $\hat{x} - x > 0$. Hence, global conditions for sliding mode are satisfied. To verify the stability of the sliding mode observer, the positive definite Lyapunov function is defined as

$$V = \frac{1}{2}(\tilde{x}_1^2 + \tilde{x}_2^2 + \tilde{x}_3^2) \tag{23}$$

The time derivative of V is defined as

$$\begin{aligned} \dot{V} &= \tilde{x}_1(\tilde{x}_2 - h_1 s - M_1 \mathrm{sgn}(s)) \\ &\quad + \tilde{x}_2\left(\frac{1}{m_v}\left[\frac{\hat{\psi}^2 - \psi^2}{2N^2\mu_0 S} - B_v\tilde{x}_2\right] - h_2 s - M_2 \mathrm{sgn}(s)\right) + \tilde{x}_3(\tilde{I}R) \\ &= (\tilde{x}_1\tilde{x}_2 - h_1\tilde{x}_1^2 - M_1 \mathrm{sgn}(s)\tilde{x}_1) \\ &\quad + \left[\tilde{x}_2\frac{1}{m_v}\left(\frac{\hat{\psi}^2 - \psi^2}{2N^2\mu_0 S} - B_v\tilde{x}_2\right) - h_2 s\tilde{x}_2 - M_2 \mathrm{sgn}(s)\tilde{x}_2 + \tilde{x}_3(\tilde{I}R)\right] \end{aligned} \tag{24}$$

Because when $\tilde{x} = \hat{x} - x < 0$, $s < 0$. when $\tilde{x} = \hat{x} - x > 0$, $s > 0$. So, it is easy to get that

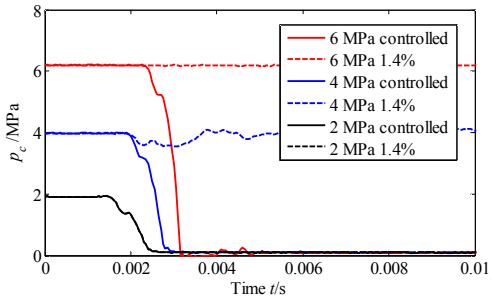

Fig. 8. Compared control pressure.

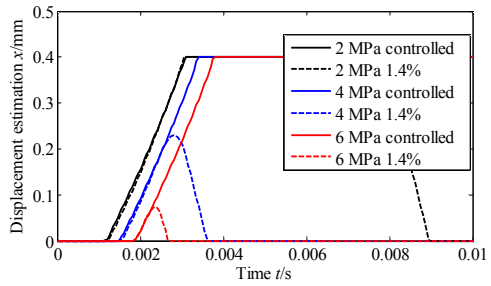

Fig. 9. Displacement estimation of ball valve.

$$\begin{aligned} \dot{V} &\le (|\tilde{x}_1||\tilde{x}_2| - h_1 s\tilde{x}_1 - M_1|\tilde{x}_1|) \\ &\quad + \left[|\tilde{x}_2|\left|\frac{1}{m_v}\left(\frac{\hat{\psi}^2 - \psi^2}{2N^2\mu_0 S} - B_v\tilde{x}_2\right)\right| - h_2 s\tilde{x}_2 - M_2|\tilde{x}_2| + |\tilde{x}_3|(\tilde{I}R)\right] \end{aligned} \tag{25}$$

When s approaches 0, $h_1 s\tilde{x}_1$ and $h_2 s\tilde{x}_2$ both converge to 0. And if M_1 and M_2 are bounded by

$$\begin{cases} M_1 \ge |\tilde{x}_2| \\ M_2 \ge \left|\dfrac{1}{m_v}\left[\dfrac{\hat{\psi}^2 - \psi^2}{2N^2\mu_0 S} - B_v\tilde{x}_2\right]\right| + \dfrac{|\tilde{x}_3|(\tilde{I}R)}{|\tilde{x}_2|} \end{cases} \tag{26}$$

Based on the above equation, we can infer that $\dot{V} < 0$ and the control system can achieve stability asymptotically.

To verify the effectiveness of the feedback controller of τ_2, a comparative study was carried out where the control pressure (p_c, Fig. 1) is analyzed for the excitation PWM signal with a fixed duty cycle (τ_2 = 1.4 %) and with a controlled duty cycle under different supply pressure. Fig. 8 shows the comparison results.

As shown in Fig. 8, for a fixed duty cycle of 1.4 %, the control pressure can only fall to 0 under the supply pressure of 2 MPa. For higher supply pressure, the HSV fails to open. However, when a feedback controller of τ_2 is implemented, control pressure can fall to 0 for even supply pressure higher than 2 MPa. This indicates that when the feedback controller is implemented, the x can reach x_{vmax} (Maximum displacement of ball valve, 0.4 mm) under different supply pressure.

Fig. 9 shows displacement estimation for a fixed duty cycle

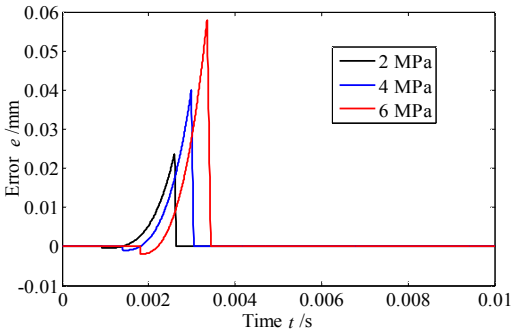

Fig. 10. Error for uncertainty in parameters under different supply pressures.

(τ_2 = 1.4 %) and for a controlled duty cycle under different supply pressure.

As shown in Fig. 9, for a fixed duty cycle, the estimated displacement of the ball valve is 0.4 mm, 0.22 mm and 0.07 mm at the supply pressure of 2 MPa, 4 MPa, and 6 MPa, respectively. This explains the change rule of the control pressure observed in Fig. 8. However, when a feedback controller of τ_2 is implemented, the estimated displacement of the ball valve is equal to 0.4 mm at the different supply pressure. Therefore, the proposed controller of τ_2 can adapt to changing supply pressure.

Since a feedback controller of τ_2 is designed based on the mathematical model of the HSV. To analyze the influences of the parametric uncertainties on the performance of the excitation PWM controller, the parameters B_v (damping coefficient of the ball valve) and R (equivalent resistance of the coil) used in the controller are considered to have a random error [34, 35].

$$B_v = 0.6+0.15\times r(t) \tag{27}$$

$$R = 10.2+2.55\times r(t) \tag{28}$$

where $r(t)$ is the normally distributed random function.

Fig. 10 shows the error (e) between the estimated displacement without uncertainties and estimated displacement with parametric uncertainties.

As shown in Fig. 10, the proposed controller is sensitive to parametric errors, and the error increases with the increasing supply pressure. But the maximum error only accounts for 10 % of the maximum displacement of the ball valve, which is acceptable in this research. Moreover, the improvement of the controller's robustness will be considered in subsequent works.

4.2 High frequency PWM

High frequency PWM is used to control the coil current in the fully-open holding stage. If τ_3 is too large, this will cause higher power consumption and higher temperature rise. Conversely, if τ_3 is too small, the ball valve cannot maintain the fully open position, which reduces the output flow rate of HSV.

To optimize the power consumption, the electromagnetic force should slightly exceed the force exerted by the supply pressure to the ball valve.

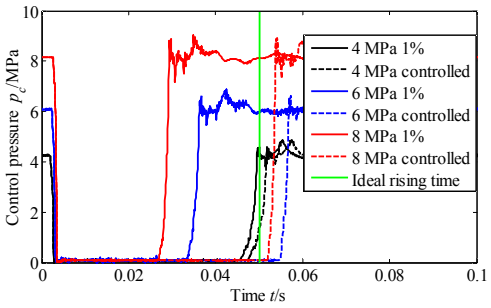

Fig. 11. Control pressure at fully-open holding stage.

When the ball valve is in the fully-open holding stage, there is a balance between critical electromagnetic force, supply pressure and steady flow force. The steady flow force is ignored due to its small value. The critical electromagnetic force is written as

$$F_{mb} = p_s A_s - F_y \tag{29}$$

Then the critical current is written as

$$I_{mb} = \frac{(L_c/u_r + (L_0 - x_{vmax}))k_f}{N}\sqrt{\frac{2(p_s A_s - F_y)}{\mu_0 S}} \tag{30}$$

Hence, the τ_3 can be written as:

$$\tau_3 = \frac{I_{mb}R}{U} \tag{31}$$

To verify the effectiveness of the feedback controller of τ_3, a comparative study was conducted where the control pressure is analyzed for the high frequency PWM signal with a fixed duty cycle (τ_3 = 1 %) and with a controlled duty cycle under different supply pressure. The duty cycle of reference PWM in this experiment is 50 % and the carrier frequency is 10 Hz. Fig. 11 shows the comparison results in which the ideal rising time refers to the time when the control pressure is expected to rise.

As shown in Fig. 11, for a fixed duty cycle τ_3 of 1 %, the control pressure rises 0.004 s ahead of the ideal rising time under the supply pressure of 4 MPa. The higher the supply pressure increases, the earlier the control pressure rises. As it can be seen from Fig. 11, the control pressure rises 0.025 s ahead of time under the supply pressure of 8 MPa, which would significantly reduce the flow rate of the HSV. This is because, with the increasing of the supply pressure, the force required to close the valve increases. However, when a feedback controller of τ_3 is implemented, the actual rising time of the control pressure is close to the ideal rising time under different supply pressure. Therefore, the proposed controller of τ_3 maintains the same fully-open holding time under different supply pressures, which proves that the proposed controller adapts to the changing supply pressure.

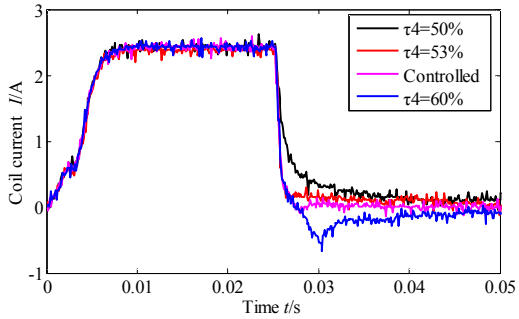

(a) Coil current

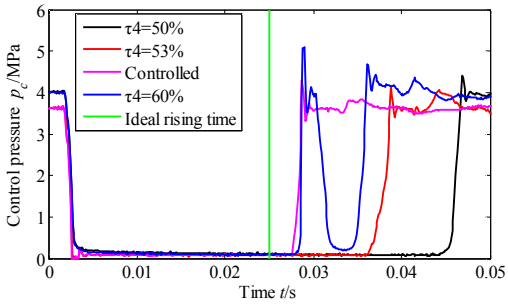

(b) Control pressure

Fig. 12. Comparison results at the carrier frequency of 20 Hz.

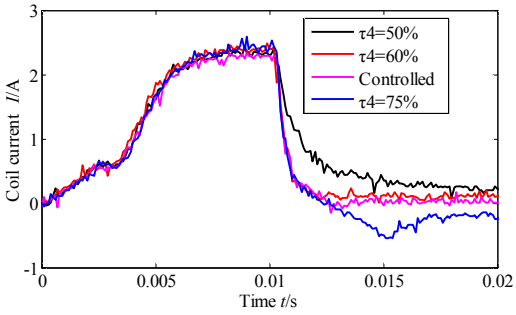

(a) Coil current

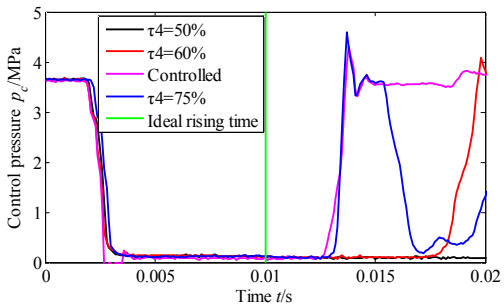

(b) Control pressure

Fig. 13. Comparison results at the carrier frequency of 50 Hz.

4.3 Reverse PWM

Reverse PWM is used to improve the unloading speed of coil current in the closing stage. The unloading speed of coil current increases with the increase of the duty cycle τ_4. Given that the electromagnetic force is positive, irrespective of the sign of the current, large duty cycle would cause the ball valve to reopen. Hence, τ_4 needs to be controlled adaptively. To optimize the duty cycle τ_4, a feedback controller for τ_4 which takes into consideration the carrier frequency of the reference PWM and the unloading time is designed as follows:

$$\tau_4 = \tau_1 + t_2 f_1 \tag{32}$$

To verify the effectiveness of the designed feedback controller of τ_4, a comparative study was carried out where coil current and control pressure are analyzed for controlled duty cycle and different fixed duty cycle of the reverse PWM at different carrier frequencies. Comparison results are shown in Figs. 12 and 13.

As shown in Fig. 12(a), for a fixed duty cycle τ_4 of 50 %, the unloading speed of the coil current is slower compared to other duty cycles. The same situation can be observed in Fig. 12(b) where the control pressure starts to increase 0.02 s after the ideal rising time. For larger duty cycles, the unloading speed of coil current increases. However, further increase of the duty cycle leads to an undesirable reestablishment of the electromagnetic force which reopens the valve. This can be seen in Fig. 12(b), where, for the duty cycle of 60 %, the control pressure rebounds. In contrast, when the duty cycle is controlled, the unloading speed is faster, the control pressure starts to rise 0.003 s after the ideal rising time and no rebound occurs. In this way, the closing stage is optimized.

For a carrier frequency of 50 Hz, the influence rule of τ_4 on coil current is the same as the previously described for a carrier frequency of 20 Hz. Except that, larger duty cycles are required to achieve the same unloading speed. Since the designed feedback controller takes into consideration the carrier frequency, the valve can maintain the same closing dynamic performance even when the carrier frequency changes.

5. Comparative experimental analysis between the adaptive PWM and the three-voltage control

To conduct a comprehensive performance comparison between the designed adaptive PWM and the three-voltage control, a test bench was set-up as shown in Fig. 14. It mainly consists of the high speed on/off valve, xPC target controller, and a hydraulic power supply. The xPC target controller is composed of a master and slave computer, data acquisition and control card (NI PCI 6251) and a power amplifier (AE Techron 7224).

Initially, the data for control pressure and coil current are collected and transferred to the PCI 6251 through the differential transfer module. Based on the Simulink model of the adaptive PWM, the slave computer process the received data to generate a PWM signal that is amplified by the power amplifier and then used to drive the HSV. The parameters of the reference PWM are pre-set. In this experiment, parameters of the three-

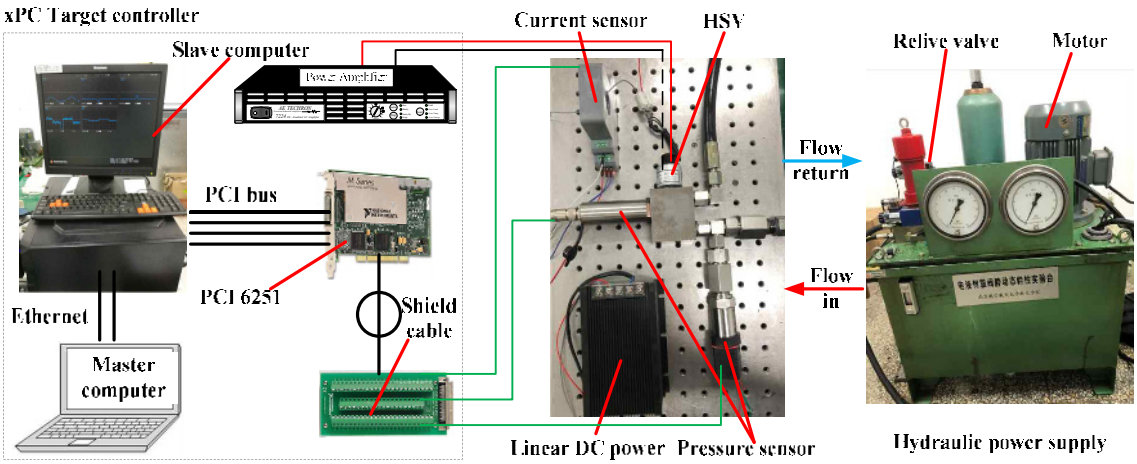

Fig. 14. Schematic diagram of test bench of the HSV.

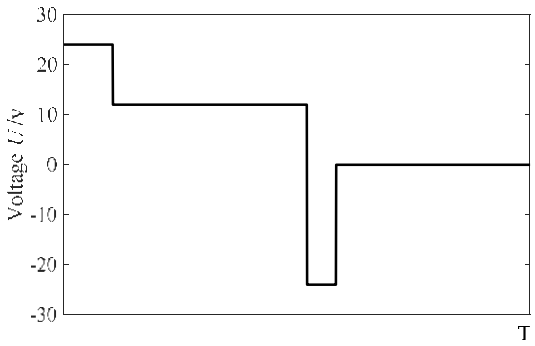

Fig. 15. Schematic diagram of the three-voltage control.

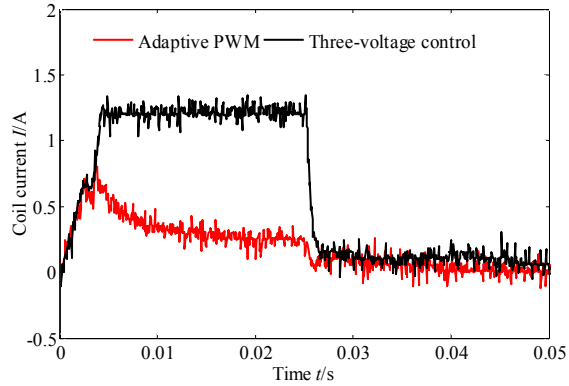

Fig. 16. Coil current of the two control strategies.

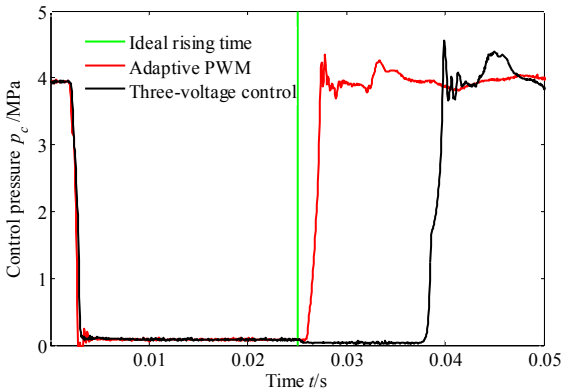

Fig. 17. Control pressure of the two control strategies.

voltage PWM signal are similar to those of the reference PWM signal for a rational comparison.

A non-contact current sensor (Ningbo Yisida NB-DI1B4-I4KD, accuracy 0.5 %, response frequency 2 kHz, range -5A~5A) was used to measure the coil current of the HSV. A high frequency pressure sensor (Kunshan Shuanqiao CYG1401F, accuracy 0.5 %, response frequency 20 kHz, range 0~10 MPa, flush type) was used to measure control pressure (p_c, Fig. 1). An infrared thermometer was used to measure temperature on the surface of the valve's coil. All of the above sensors were powered by a linear DC power supplier (Chaoyang Power 4NIC-X24, output power 24 V, and ripple wave less than 1 mV).

5.1 Dynamic performance

To compare the dynamic performance between adaptive PWM control and three-voltage control (Fig. 15, the amplitudes of the three voltage are set to be fixed value), a dynamic test of the HSV was implemented under a specific condition (carrier frequency of the reference PWM signal is 20 Hz and duty cycle τ_1 is 50 %). Figs. 16 and 17 show the comparative results of coil current and control pressure under the two control strategies.

As shown in Fig. 16, in the closing stage, with the three-voltage control, the unloading speed of the coil current is relatively slow compared to the unloading speed with the adaptive PWM control. Conversely, for an adaptive PWM control, the high frequency PWM maintains the coil current slightly above the critical current; and once the reverse PWM is applied the unloading time is shorter because the amplitude of the coil current used to hold the fully-open position is lower in the adap-

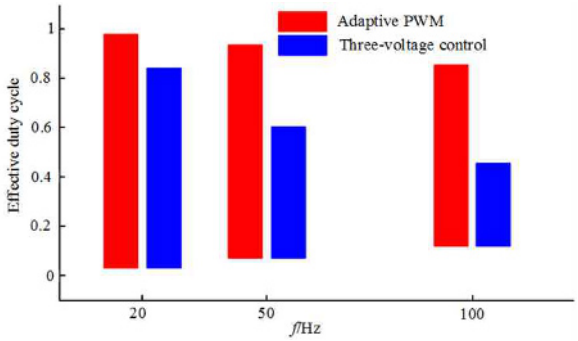

Fig. 18. The effective range of duty cycle at different carrier frequencies under 4 Mpa.

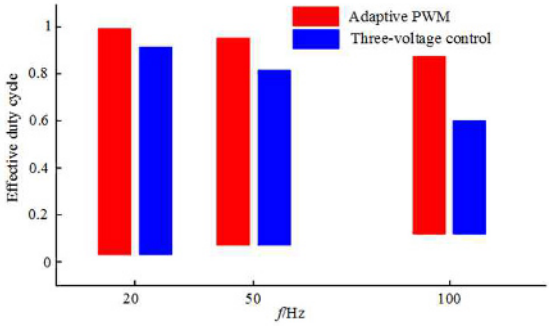

Fig. 19. The effective range of duty cycle at different carrier frequencies under 6 Mpa.

tive PWM control strategy.

As shown in Fig. 17, compared to the three-voltage control, the rising delay time of the control pressure drastically reduces by 84.6 % (from 13 ms to 2 ms) with the adaptive PWM control. This clearly shows how the dynamic performance is greatly improved by the proposed adaptive PWM control strategy.

5.2 Static performance

The relationship between flow rate and duty cycle is often used to assess the static performance of HSV. Key parameters that determine the static performance are dead band, effective range, and saturation of the valve's duty cycle. The performance is improved by enlarging the effective range of the valve. Therefore, to compare the static performance between adaptive PWM control and three-voltage control, a static test of HSV was conducted at different frequencies and different supply pressures.

The comparative bar charts of the duty cycle's effective ranges of the two control strategies, under supply pressure of 4 MPa and 6 MPa, are as shown in Figs. 18 and 19.

It can be seen from Figs. 18 and 19 that the effective range of duty cycle decreases with the increasing carrier frequency. When the carrier frequency reaches 100 Hz, the duty cycle's effective range with the three-voltage is narrow (12 %-45 %), under the supply pressure of 4 MPa. In contrast, the HSV controlled by the adaptive PWM can still achieve better static performance since the duty cycle's effective range increases by 121 % (12 %-85 %), compared to the three-voltage controller.

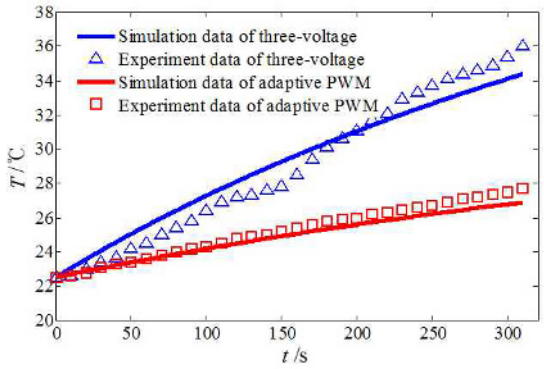

Fig. 20. Compared temperature rise.

As shown in Fig. 19, with the three-voltage controller, caused by increased supply pressure, the movement resistance of the ball valve increases and leads to the enlargement of the dead band range and the shrinkage of the effective range. However, with the adaptive PWM control, the increase of the supply pressure barely affects the effective range. For example, at the carrier frequency of 50 Hz, when the supply pressure is increased to 6 MPa, the effective range of the HSV controlled by the three-voltage is greatly affected. Therefore, in addition to increasing the frequency bandwidth of the HSV, the proposed adaptive PWM is proved to be stable and robust.

5.3 Temperature rise

To compare the temperature rise of the adaptive PWM and the three-voltage control, an infrared thermometer was used to measure temperature on the surface of the valve's coil shell under an ambient temperature of 22.5 °C. To save experimental time, the experiment was conducted with the adaptive PWM before conducting it with the three-voltage, since it was predicted that the valve experiences significant temperature rise when the three-voltage is used. The duration of each experiment is 310 s. Fig. 20 shows the comparative results.

The experimental results basically agree with the simulation results, which validates the accuracy of the temperature model. The experimental results also indicate that when adaptive PWM control is used, the temperature rise is reduced by 61.5 %, compared to the three-voltage control. This is due the excitation PWM that limits the maximum value of the coil current in the opening stage, and the high frequency PWM that holds the optimal value of the coil current in the fully-open holding stage.

6. Conclusion

A new adaptive PWM control method for HSV is proposed, and its working principle is presented. The proposed adaptive PWM consists of a reference PWM, an excitation PWM, a high frequency PWM, and a reverse PWM whose logical sequence

is controlled.

To improve the performance of the HSV:

(1) An excitation PWM with a feedback controller based on sliding mode observer is proposed to ensure that the ball valve can reach the maximum opening position even under different supply pressures. The experimental results indicate that the estimated displacement of the ball valve reaches the maximum at different supply pressures. Therefore, the excitation PWM adapts to the changing supply pressure.

(2) A high frequency PWM with a feedback controller based on supply pressure is proposed to optimize the coil current in the fully-open holding stage. The experimental results indicate that the actual rising time of the control pressure is close to the ideal rising time under different supply pressures. Therefore, the high frequency PWM adapts to the changing supply pressure and maintains the accuracy of HSV's average flow rate.

(3) A reverse PWM with a feedback controller based on unloading time of the coil current is proposed to overcome the influence of the inductance in the closing stage. The experimental results indicate that the valve can maintain the same closing dynamic performance even when the carrier frequency changes.

(4) Comparative experimental results demonstrated that, with the proposed adaptive PWM control, the rising delay time of the control pressure drastically reduces by 84.6 % (from 13 ms to 2 ms); the HSV can still achieve better static performance compared to the three-voltage control, since the duty cycle's effective range is large (12 %-85 %) even with a higher carrier frequency (100 Hz); and the temperature rise of the valve's coil shell is reduced by 61.5 %, compared to the three-voltage control.

Acknowledgments

This work was supported by the National Natural Science Foundation of China (grant number 51975275, 51575258).

References

[1] S. Wu, X. Y. Zhao, C. F. Li, Z. X. Jiao and F. Qu, Multi-objective optimization of a hollow plunger type solenoid for high speed on/off valve, *IEEE Transactions on Industrial Electronics*, 65 (4) (2018) 3115-3124.

[2] H. Y. Yang and M Pan, Engineering research in fluid power: A review, *J. of Zhejiang University Science A*, 16 (6) (2015) 427-442.

[3] M. S. A. Laamanen and M. Vilenius, Is it time for digital hydraulics? *The Eight Scandinavian International Conference on Fluid Power, Proceedings of the Conference*, May 7-9, Tampere, Finland, Tampere University of Technology (2003) 347-366.

[4] R. Scheidl, M. Linjama and S. Schmidt, Is the future of fluid power digital, *Proceedings of the Institution of Mechanical Engineers Part I, J. of Systems & Control Engineering*, 226 (6) (2012) 721-723.

[5] M. Pan and A. Plummer, Digital switched hydraulics, *Frontiers of Mechanical Engineering*, 13 (2) (2018) 225-231.

[6] R. Brandstetter, T. Deubel, R. Scheidl, B. Winkle and K. Zeman, Digital hydraulics and "Industrie 4.0", *Proceedings of the Institution of Mechanical Engineers Part I J. of Systems & Control Engineering*, 231 (2) (2017) 82-93.

[7] M. Paloniitty, M. Linjama and K. Huhtala, Equal coded digital hydraulic valve system–improving tracking control with pulse frequency modulation, *Procedia Engineering*, 106 (2015) 83-91.

[8] M. Linjama and M. Vilenius, Digital hydraulics-Towards perfect valve technology, *The Tenth Scandinavian International Conference on Fluid Power (SICFP'07)*, May 21-23, Tampere, Finland (2007).

[9] M. Linjama, Digital fluid power: State of the art, *12th Scandinavian International Conference on Fluid Power*, Tampere, Finland, May (2011) 18-20.

[10] M. Paloniitty and M. Linjama, High-linear digital hydraulic valve control by an equal coded valve system and novel switching schemes, *Proceedings of the Institution of Mechanical Engineers Part I J. of Systems & Control Engineering*, 232 (3) (2018) 258-269.

[11] H. Y. Yang, S. Wang, B. Zhang, H. C. Hong and Q. Zhong, Development and prospect of digital hydraulic valve and valve control system, *J. of Jilin University (Engineering and Technology Edition),* 46 (5) (2016) 1494-1505.

[12] Z. X. Jiao, X. C. Liu, Y. X. Shang and C. Huang, An integrated self-energized brake system for aircrafts based on a switching valve control, *Aerospace Science & Technology*, 60 (2017) 20-30.

[13] A. H. Meng and J. Song, Linear control performance improvement of high speed on-off valve controlled by PWM, *SAE International J. of Commercial Vehicles*, 8 (2015) 283-292.

[14] H. B. Jian, J. Ruan and S. Li, Design and experiment of 2D electrohydraulic high-speed on-off valve, *Transactions of the Chinese Society of Agricultural*, 46 (2) (2015) 328-334.

[15] J. Man, F. Ding, Q. Li and J. Da, Novel high-speed electromagnetic actuator with permanent-magnet shielding for high-pressure applications, *IEEE Transactions on Magnetics*, 46 (12) (2010) 4030-4033.

[16] X. W. Kong and S. Z. Li, Dynamic performance of high speed solenoid valve with parallel coils, *Chinese J. of Mechanical Engineering*, 27 (4) (2014) 816-821.

[17] Y. P. Shi, C. W. Liu and Y. Zhang, Design and study of a new kind of larger flow rate high-speed on-off valve, *Chinese J. of Mechanical Engineering*, 40 (4) (2004) 195-198.

[18] C. Zhou, J. Duan, G. L. Deng and J. Li, A novel high-speed jet dispenser driven by double piezoelectric stacks, *IEEE Transactions on Industrial Electronics*, 64 (1) (2017) 412-419.

[19] N. Bruno, Y. Zhu, C. Liu, Q. Gao and Y. Li, Development of a piezoelectric high speed on/off valve and its application to pneumatic closed-loop position control system, *J. of Mechanical Science and Technology*, 33 (6) (2019) 2747-2759.

[20] Q. Wang, F. Yang, Y. Qian, J. Chen and H. Guan, Experimental analysis of new high-speed powerful digital solenoid valves, *Energy Conversion & Management*, 52 (5) (2011) 2309-2313.

[21] Q. Cheng, Z. Zhang and N. Xie, Power losses analysis of the gasoline direct injector within different driven strategies, *International J. of Applied Electromagnetics & Mechanics*, 50 (3) (2016) 379-394.
[22] R. Goraj, Impact of the pulse width modulation on the temperature distribution in the armature of a solenoid valve, *International J. of Applied Mechanics & Engineering*, 20 (4) (2015) 773-786.
[23] J. Zhao, M. Wang, Z. Wang, G. Lenoid, Q. Tao and X. Ma, A different boost voltage effects on the dynamic response and energy losses of high-speed solenoid valves, *Applied Thermal Engineering*, 123 (2017) 1494-1503.
[24] J. Zhao et al., Hold current effects on the power losses of high-speed solenoid valve for common rail injector, *Applied Thermal Engineering*, 128 (2018) 1579-1587.
[25] M. Heikkilä, M. Paloniitty and M. Linjama, Fast switching valve for low-pressure water hydraulic, *Proceedings of the Ninth Workshop on Digital Fluid Power*, September 7-8, Aalborg, Denmark (2017).
[26] I. Y. Lee, Switching response improvement of a high speed on/off solenoid valve by using a 3 power source type valve driving circuit, *IEEE International Conference on Industrial Technology,* IEEE (2006) 1823-1828.
[27] A. Plöckinger, R. Scheidl and B. Winker, Performance, durability and applications of a fast switching valve, *The Second Workshop on Digital Fluid Power*, DFP'09, ISBN 978-3-200-01713-9, November 12-13, Linz, Austria (2009).
[28] M. Linjama et al., Mechatronic design of digital hydraulic micro valve package, *Procedia Engineering*, 106 (2015) 97-107.
[29] Q. Zhong, B. Zhang, H. C. Hong and H. Y. Yang, Three power sources excitation on control strategy of high speed on/off valve based on current feedback, *J. of Zhejiang University: Engineering Science*, 52 (1) (2018) 8-15.
[30] Q. Zhong, B. Zhang, H. Y. Yang, J. E. Ma and R. F. Fung, Performance analysis of a high-speed on/off valve based on an intelligent pulse-width modulation control, *Advances in Mechanical Engineering*, 9 (11) (2017) 1-11.
[31] M. Taghizadeh, A. Ghaffari and F. Najafi, Modeling and identification of a solenoid valve for PWM control applications, *Comptes Rendus Mecanique*, 337 (3) (2009) 131-140.
[32] C. M. Wang, C. Sha and X. F. Wei, Temperature increment research of DC solenoid valve, *Chinese Hydraulics & Pneumatics*, 8 (2014) 60-63 (in Chinese).
[33] C. G. Deng and Z. Q. Xiang, Sensorless control of high-speed dot-matrix pulse jet generator, *Optics and Precision Engineering*, 20 (4) (2012) 752-759.
[34] J. M. Balthazar, A. M. Tusset, S. L. T. De Souza and A. M. Bueno, Microcantilever chaotic motion suppression in tapping mode atomic force microscope, *Proceedings of the Institution of Mechanical Engineers, Part C: J. of Mechanical Engineering Science*, 227 (8) (2013) 1730-1741.
[35] N. J. Peruzzi, F. R. Chavarette, J. M. Balthazar, A. M. Tusset, A. L. P. M. Perticarrari and R. M. F. L. Brasil, The dynamic behavior of a parametrically excited time-periodic MEMS taking into account parametric errors, *J. of Vibration and Control*, 22 (20) (2016) 4101-4110.

Qiang Gao received the B.S. in 2014 in Mechanical Engineering at Nanjing Institute of Technology and received the M.S. in 2017 in Mechanical Engineering at Yanshan University. He is currently a Ph.D. candidate in the College of Mechanical and Electrical Engineering at Nanjing University of Aeronautics and Astronautics. His research interests are digital hydraulics and smart materials.

Yuchuan Zhu is currently a Professor at National Key Laboratory of Science and Technology on Helicopter Transmission, Nanjing University of Aeronautics and Astronautics, Nanjing, China. He received the M.S. from Anhui University of Science and Technology, Huainan, China, in 2003 and the Ph.D. from Nanjing University of Science and Technology, Nanjing, China, in 2007. His research interests include smart material and structure technology, and fluid power transmission and control.

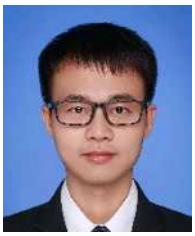

Zhang Luo received the B.S. in Mechanical Engineering from Taiyuan University of Technology, Taiyuan, China, in 2014 and the M.S. in Mechanical Engineering from Nanjing University of Aeronautics and Astronautics, Jiangsu, China, in 2019. His research interests include High speed on/off valve and smart materials.

Niyomwungeri Bruno received the B.S. in Mechanical Engineering from the University of Rwanda, Kigali, Rwanda, in 2015 and he is currently pursuing the M.S. in Mechatronic Engineering at Nanjing University of Aeronautics and Astronautics, Nanjing, China. His research interests include smart materials-based actuators and digital fluid power systems.